Inorganic Chemistry

Article

pubs.acs.org/IC

Influence of Aqueous Precursor Chemistry on the Growth Process of Epitaxial $SrTiO_3$ Buffer Layers

Glenn Pollefeyt,[†] Sander Clerick,[†] Pieter Vermeir,[‡] Petra Lommens,[†] Klaartje De Buysser,[†] and Isabel Van Driessche*[,†]

[†] SCRiPTS, Department of Inorganic and Physical Chemistry, Ghent University, Krijgslaan 281-S3, 9000 Gent, Belgium

[‡] INKAT, Department of Industrial Technology and Construction, Ghent University, Valentin Vaerwyckweg 1, 9000 Gent, Belgium

Supporting Information

ABSTRACT: In this Article, epitaxial thin films of $SrTiO_3$ were prepared on single crystalline (100) $LaAlO_3$ by an aqueous chemical solution deposition method. By using different chelating agents to stabilize the metal ions in water, the impact of the precursor chemistry on the microstructural and crystalline properties of the films was studied. Thorough investigation of the precursor by means of infrared and Raman spectroscopy as well as thermogravimetric analysis revealed that stable precursors can be obtained in which strontium ions can be either free in the solution or stabilized by one of the chelating agents. This stabilization of strontium ions appeared to be essential in order to obtain single phase $SrTiO_3$ films. Precursors in which Sr^{2+} remained as free ions showed SrO microcrystal segregation. Precursors in which both metal ions were stabilized gave rise to strongly textured, dense, and terraced $SrTiO_3$ films, allowing subsequent deposition of $YBa_2Cu_3O_{7-\delta}$ with superior superconducting performances.

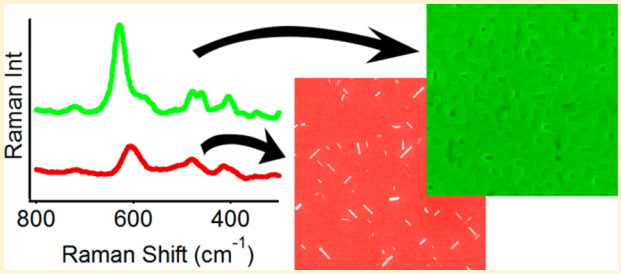

1. INTRODUCTION

In recent years, thin films of $SrTiO_3$ (STO) have been widely studied due to their applicability in various fields. $SrTiO_3$ exhibits the perovskite crystal structure with a unit-cell parameter of a = 0.3905 nm and behaves as a semiconductor with a band gap of 3.2 eV.[1] Due to the high charge storage capacity (i.e., dielectric constant), good insulating properties, chemical stability, and nontoxicity, the applications of STO thin films range from multifunctional devices such as high density capacitors, nonvolatile memories, and electro-optic components to buffer layers for superconducting coated conductors.[2−7] These conductors generally consist of a textured or polycrystalline metallic substrate, a stack of textured buffer layers, and a superconducting $YBa_2Cu_3O_{7-\delta}$ layer capped with a protective layer.[8,9] Titanate materials such as $SrTiO_3$ exhibit a small oxygen diffusion coefficient and a good chemical stability toward both the metallic substrate and the superconducting film, making these materials an interesting alternative for the commonly used buffer layers.[6,10] The current publication relates to the applicability of $SrTiO_3$ as a single buffer layer for obtaining optimal superconducting properties of $YBa_2Cu_3O_{7-\delta}$ coatings, but the results will be generic in nature.

For all of the applications stated above, the perovskite thin films have to exhibit certain crystalline and morphological properties, leading to a higher degree of interest for textured STO films over those of polycrystalline or amorphous nature.[11−13] Moreover, to use $SrTiO_3$ as a buffer layer for high temperature superconductors, the synthesis has to be compatible with the used metal substrates, leading to processing conditions in which very low oxygen partial pressures or reducing atmospheres are used.[6,10] Up to now, these crystalline properties were obtained by depositing $SrTiO_3$ via vacuum deposition techniques such as physical vapor deposition (PVD), pulsed laser deposition (PLD), RF sputtering, or molecular beam epitaxy (MBE).[12−14] However, in the past decade, chemical solution deposition (CSD) received growing attention as a promising technique for the deposition of ceramic thin films. In contrast to the above-noted vacuum techniques, CSD-methods offer the advantage of high yields, high speeds, low cost, and easy processing routes.[6,9,15]

Typically, chemical solution deposition of perovskite STO thin films consists of mixing strontium and titanium alkoxides under water-free conditions as most commercially available titanium precursors are extremely sensitive for hydrolysis, leading to $Ti(OH)_4$ precipitation upon contact with water.[10,16] Compounds such as methanol, 2-methoxyethanol, or methoxypropanol are then used as solvent. Chelation of the starting materials with compounds such as (glacial) acetic acid for the strontium ions and acetylacetone for the titanium ions to reduce the hydrolysis sensitivity results in solutions which are slightly easier to handle in open air.[3,4,16,17] Furthermore, the stabilization of the metal ions can lead to an improved growth mechanism, leading to films of higher quality.[3]

Nevertheless, in view of sustainable development and conservation of the environment, chemical solution deposition

Received: December 13, 2013
Published: April 29, 2014

   dx.doi.org/10.1021/ic403067h | Inorg. Chem. 2014, 53, 4913−4921

methods are now shifting from these toxic and/or corrosive conventional manufacturing processes toward alternative aqueous-based solution routes for the synthesis of modern functional materials.[18] However, the hydrolysis sensitivity of elements such as titanium strongly hampers the development of inorganic materials from aqueous solutions. To bypass this problem and to ensure compatibility of the metal ions with water, they are again stabilized with various complexing agents, giving rise to water-insensitive metal−chelate complexes and precursor solutions which can be stable for over months or even years.[9,18,19] A high diversity of methods and solutions can be found for various materials such as TiO_2,[19,20] $BaTiO_3$,[21] $La_2Zr_2O_7$,[22,23] CeO_2,[24,25] $YBa_2Cu_3O_{7-\delta}$,[26,27] and $YBiO_3$.[8] Nevertheless, a general synthesis approach or proper investigation toward the influence of the precursor chemistry on the final film properties in water-based systems has only barely been reported. Most of these studies consist of varying the complexing agent for monometallic systems, which can lead to major changes in the obtained decomposition behavior, crystallinity, and morphology of the films.[28−31] From these studies, which show similar conclusions as for the organic-based synthesis, it is clear that optimizing the precursor chemistry is essential for obtaining high quality ceramic films.

In this study, multiple new water-based $SrTiO_3$ precursor solutions were developed and analyzed by means of TGA−DTA, ATR-FTIR, and Raman spectroscopy. Subsequently, all solutions were coated onto single crystalline $LaAlO_3$ (100) and processed in metal-compatible conditions in order to investigate the influence of various complexing agents in the aqueous solutions on the final morphological and crystalline properties of the obtained STO films.

2. EXPERIMENTAL SECTION

2.1. Solution Preparation. To study the influence of the precursor chemistry on the final properties of the obtained $SrTiO_3$ film, four novel water-based precursor systems were developed. These solutions consist of combinations of two Sr^{2+} solutions and two Ti^{4+} solutions, all in aqueous conditions. For the strontium solutions, iminodiacetic acid (IDA, Alfa Aesar >98%) or ethylenediaminetetraacetic acid (EDTA, Sigma-Aldrich 99.4%−100.6%) was dissolved in water with a molar ratio of, respectively, 2:1 and 1:1 relative to Sr^{2+} by addition of 1.5 mL of ethanolamine (EA, Fluka >99.0%). After complete dissolution of the complexing agents, $Sr(NO_3)_2$ (Sigma-Aldrich, > 99.0%) was added to obtain a stable 0.7 M Sr^{2+} precursor with a pH of about 8.

For the Ti^{4+} solutions, two different pathways were followed. For the first type of precursor, titanium-isopropoxide was precipitated in a 10-fold of water, and the precipitate was filtered and washed to obtain wet $Ti(OH)_4$,[30] which was then redissolved in a mixture of H_2O_2 (Sigma-Aldrich 35 wt % in H_2O), IDA, and water. Both hydrogen peroxide and IDA were used in a 2:1 ratio relative to the titanium concentration. After addition of ethanolamine and 1 h of stirring at 60 °C, a stable 0.7 M titanium stock solution with a pH of 4 was obtained.

For the second type of Ti^{4+} solutions, titanium-isopropoxide was added to triethanolamine (TEA, Roth, >99%) in a 2:1 ratio with respect to the metal ion. After stirring of this mixture, hydrogen peroxide (2:1 to Ti^{4+}) and water are added giving rise to a stable precursor solution with a metal concentration of 0.7 M and a pH of around 8.5.

In order to obtain $SrTiO_3$ precursor solutions exhibiting long-term stability, stoichiometric amounts of the obtained single metal precursors were mixed, and their pH was adjusted to 5 or 7 by addition of HNO_3 (Roth, 65 wt % in H_2O) as shown in Table 1.

In aqueous chemical solution deposition processing, the formation of stable metal chelates is known to be dominated by equilibrium reactions characterized by their stability constants. Due to these equilibria, it is likely that ligands which were initially bound to strontium ions switch to the titanium ions and vice versa. In order to study these ligand exchanges by Raman and infrared measurements, additional metal solutions were prepared. A strontium−TEA solution was obtained by dissolving TEA in water with a molar ratio of 2:1 with respect to Sr^{2+}. After addition of $Sr(NO_3)_2$, a stable 0.7 M Sr−TEA precursor was obtained with a pH of around 7. An additional titanium−EDTA solution was also prepared by replacing IDA in the above-described method by EDTA in a 1:1 molar ratio, leading to a stable 0.7 M Ti−EDTA solution with a pH of 4.

Table 1. List of $SrTiO_3$ Solutions

name	Sr^{2+} complex	Ti^{4+} complex	pH	concentration
IDA−IDA	IDA	IDA−H_2O_2	5	0.7 M
IDA−TEA	IDA	TEA−H_2O_2	7[a]	0.7 M
EDTA−TEA	EDTA	TEA−H_2O_2	5	0.7 M
EDTA−IDA	EDTA	IDA−H_2O_2	5	0.7 M

[a]The pH was set to 7 as the solution was unstable at pH 5.

To study the stability of the precursors at higher temperatures, all the solutions were gelled at 60 °C for 4 h in a drying furnace. Throughout this gelation step, most of the solvent evaporates, and a highly viscous substance is obtained. The stability of this gel is essential for obtaining compositional homogeneity throughout the film. Only the monometallic Sr−TEA and the bimetallic TEA−IDA solutions showed precipitation leading to inhomogeneous gels.

In order to identify precursor-characteristic vibrations in the Raman and infrared measurements, metal-ion free blanks were also synthesized.

2.2. Thin Film Deposition and Thermal Processing. The STO solutions were coated on polished (100)-$LaAlO_3$ single crystals (Crystek GmbH) by means of dip-coating or DOD piezoelectric inkjet printing (Microfab). Experimental conditions concerning the inkjet deposition are reported elsewhere.[26] Prior to coating, the substrates were rinsed with isopropanol and heated to 400 °C in order to remove adsorbed organics.[32] After cooling the substrate to room temperature, the solution was coated onto the substrate with suitable conditions and speeds in order to obtain 100−150 nm thick films.

The as-coated films were first dried in a drying furnace at 60 °C for 30 min. The high temperature synthesis of these dried films was performed in a quartz tube furnace under controlled dry or humid Ar/5% H_2 atmosphere. This atmosphere was chosen in order to preserve compatibility of the processing conditions with commonly used metallic substrates in the superconducting coated conductor architectures, the final goal of this research. To obtain a humid atmosphere, the forming gas was bubbled through two water bubblers at room temperature. The dried films were heated with a heating rate of 8 °C/min to 1100 °C for 2 h and furnace-cooled afterward. The flow of the (humid) forming gas was kept constant at 150 mL/min. As a reference, some of the sintered films were postannealed in pure oxygen at 1100 °C for 2 h. The oxygen partial pressure during processing was monitored via a DS oxygen probe from Australian Oxytrol Systems.

For the YBCO deposition, pulsed laser deposition was performed at 810 °C and an oxygen background pressure of 0.3 mbar.[33] A KrF excimer laser was used, applying 3000 pulses on the YBCO target with a repetition rate of 5 Hz to deposit a 200 nm thick film. The samples were cooled down and oxygenated in an oxygen partial pressure of 0.4 bar.

2.3. Characterization. Characterization of the single metal and STO precursors was performed by both ATR-FTIR (PerkinElmer Spectrum 100) and dispersive Raman spectroscopy (RamanRxn, Kaiser Optical Systems Inc., 532 nm). For the ATR-FTIR measurements, gels of both the metal containing solutions and their blanks were measured in open air. In the case of the Sr−TEA and TEA−IDA precursors, solutions were measured as the gels were unstable. For Raman spectroscopy, the precursor solutions were measured as-synthesized, since the Raman signal showed high fluorescence in the gel phase, due to the strong orange-brown color of the gels. Thermal

dx.doi.org/10.1021/ic403067h | Inorg. Chem. 2014, 53, 4913−4921

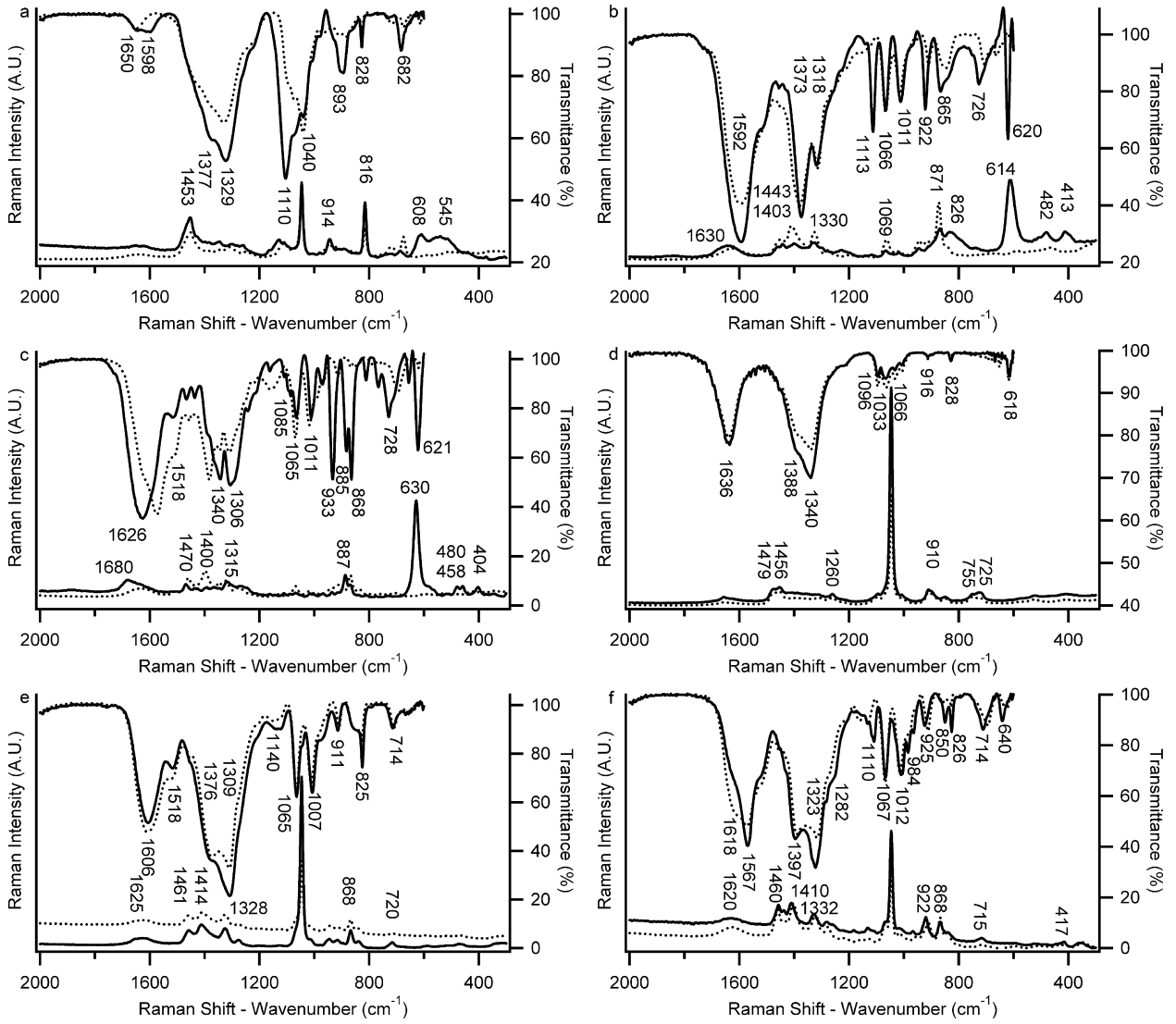

Figure 1. Infrared (top, right axis) and Raman (bottom, left axis) spectra of monometallic precursors (—) and their blanks (---): Ti−TEA (a), Ti−IDA (b), Ti−EDTA (c), Sr−TEA (d), Sr−IDA (e), and Sr−EDTA(f).

analysis of the precursors was performed with a Netzsch STA 449 F3 Jupiter with a heating rate of 10 °C/min and an air flow rate of 120 mL/min.

Characterization of the texture and phase composition of the $SrTiO_3$ films was performed by means of X-ray diffraction (Siemens D5000 diffractometer). Structural characterization was carried out with a FEI Nova 600 Nanolab Dual Beam FIB-SEM and a JEOL JSM-7600F. Roughness analysis of the thin films was carried out by atomic force microscopy (Molecular Imaging PicoPlus) operating in tapping mode with Budgetsensors Tap 300 tips and post processed with WSxM software.[34] XPS measurements were recorded on a S-probe XPS spectrometer with monochromatic Al Kα radiation from Surface Science Instruments (VG). Sputtering of the films was performed with an Ar^+ ion gun at 4 kV. A nickel grid placed 3 mm above the sample was used to suppress charging effects. Experimental data were processed using the software package CasaXPS (Casa Software Ltd., U.K.). The quality of the deposited YBCO layers was determined with inductive measurements of the critical current density J_c (CryoscanTM by THEVA).

3. RESULTS AND DISCUSSION

3.1. Precursor Analysis. In Figure 1, the infrared and Raman spectra of the monometallic precursors are shown in the fingerprint area ranging from 2000 to 300 cm^{-1}. These spectra are compared to those obtained for their metal-ion free blanks, in order to identify characteristic vibrations of the formed metal−chelates. The assignment of the various absorption bands and Raman shifts according to literature is shown in Table 2 (Supporting Information).[28,29,35−37]

In the case of the Ti−TEA precursor (Figure 1a), four characteristic vibrations appear at 1598, 1110, 893, and 682 cm^{-1} while these are absent in the spectrum of the blank. The strongest absorbances at 1110 and 893 cm^{-1} can be assigned to, respectively, the C−N(−C) stretch of TEA and the O−O stretch of H_2O_2, both coordinated to the metal ion. The chelating reaction of TEA (and H_2O_2) with the Ti^{4+} ion can also be observed in the Raman spectra, where 3 Raman shifts appear at 1130, 608, and 545 cm^{-1} upon addition of titanium to the blank. These shifts can, respectively, be attributed to the C−N(−C) stretch of TEA and M−O, M−N, or skeletal ligand shell vibrations. Additional shifts of the spectra in both the infrared and Raman spectrum can be attributed to the chelating effect of the triethanolamine, which in turn has an influence on the total vibrational and electronic states of the molecule.

dx.doi.org/10.1021/ic403067h | Inorg. Chem. 2014, 53, 4913−4921

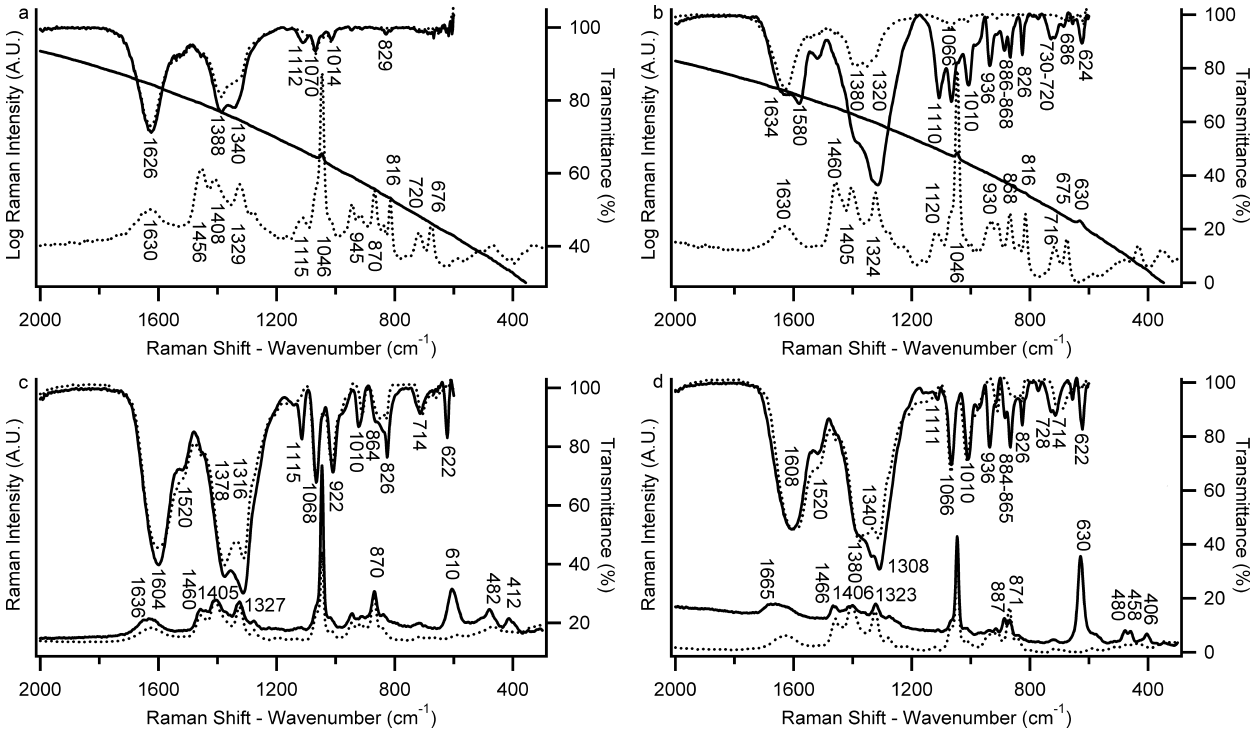

Figure 2. Infrared (top, right axis) and Raman (bottom, left axis) spectra of bimetallic precursors: Sr−IDA−Ti−TEA (a), Sr−EDTA−Ti−TEA (b), Sr−IDA−Ti−IDA (c), and Sr−EDTA−Ti−IDA (d).

For the Ti−IDA precursor (Figure 1b), the metal coordinated C−N(−C) stretch can again be observed at 1110 cm^{-1} as well as additional bands at 922, 865, and 620 cm^{-1}. The band at 922 cm^{-1} can be assigned to the C−O deformation of IDA's coordinated carboxylate ions, whereas the band at 865 cm^{-1} can be attributed to the O−O stretch of H_2O_2 coordinated to Ti^{4+}. The $\upsilon_{as}(Ti-O_2)$ can be observed in both the infrared (620 cm^{-1}) and the Raman spectrum (614 cm^{-1}). Furthermore, additional Ti−N or skeletal motions of the chelated site can be observed in the Raman spectrum at 482 and 413 cm^{-1}. Apart from these direct metal−ligand motions, also the vibrational modes of carboxylate groups are strongly dependent on their chelating behavior. Only small shifts of both the symmetric and asymmetric COO^- stretches are observed with slightly higher energy difference ($\Delta\upsilon$) in both the Raman and infrared spectrum, indicating the presence of bridging carboxylate groups.[35]

In the case of the Ti−EDTA precursor (Figure 1c), clear shifts of the carboxylate's vibrational modes toward a higher $\Delta\upsilon$ of 185 cm^{-1} with respect to the free carboxylate can be seen, indicating the monodentate bonding behavior of the chelating COO^- groups.[35] These shifts can be seen in both the infrared and the Raman spectrum, although it is worth noting that the symmetric stretch is almost absent in the Raman spectrum. This feature can also be attributed to the monodentate bonding behavior, leading to a decreased polarizability and subsequent Raman sensitivity of the symmetric carboxylate stretch. Next to the shifted carboxylate peaks, additional infrared absorptions are found at 933 cm^{-1} (π(C−O)), a doublet around 870 cm^{-1}(υ(O−O), υ_s(C−N)), and 621 cm^{-1} ($\upsilon_{as}(Ti-O_2)$). The C−N(−C) stretch which was observed at 1110 cm^{-1} for both the TEA and IDA containing precursors has now split into a weaker doublet with peaks at 1110 and 1085 cm^{-1}, which can most likely be attributed to the higher symmetry of the chelating agent. As for the other titanium precursors, additional vibrational motions are observed in Raman below 650 cm^{-1}, with a very strong $\upsilon_{as}(Ti-O_2)$ vibrational mode at 630 cm^{-1}.

In contrast to the previous Ti^{4+} precursors, the Sr−IDA and Sr−TEA precursors show no clear differences with respect to their metal-ion free blanks (Figure 1d,e), indicating that both iminodiacetic acid and triethanolamine have no interaction with the Sr^{2+} ion. The higher intensity of the infrared band at 1330−1340 cm^{-1} and Raman scattering at 1046 cm^{-1} can be assigned to the higher concentration of NO_3^- groups, as strontium nitrate was used as metal salt to prepare the solutions. For the Sr−EDTA (Figure 1f) precursor, no clear shifts of the carboxylate stretches are observed in both the infrared and Raman spectrum. Furthermore, only one (weak) characteristic motion is observed in the low frequency Raman spectrum at 417 cm^{-1}. This vibrational mode can most likely be assigned to the stretching of the Sr−N bond. The existence of this bond is also demonstrated by the presence of the coordinated C−N(−C) stretch at 1110 cm^{-1}. From these measurements, it can be concluded that EDTA solely bonds through the nitrogen atoms with the strontium ions. This preferred bonding of strontium with nitrogen can be expected from the hard soft acid base principle, as strontium is a soft acid and nitrogen is a softer base than oxygen.

These results are in good agreement with the theoretical stability constants of the metal−chelate formation, as it is generally known that EDTA is a stronger chelating agent than TEA and IDA.[38−41]

In order to obtain precursors suitable for the deposition of $SrTiO_3$ films, stoichiometric amounts of the Sr^{2+} and the Ti^{4+} precursors are mixed leading to STO precursors. Upon this mixing, the differences in chelating strength of the used ligands are the driving force for possible ligand exchanges. To study these phenomena, the obtained bimetallic precursors and their

dx.doi.org/10.1021/ic403067h | Inorg. Chem. 2014, 53, 4913−4921

metal-ion-free blanks were again examined by both Raman and infrared spectroscopy, as shown in Figure 2.

It can be seen that the Raman spectrum of the TEA−IDA precursor (Figure 2a) suffers from Raman fluorescence, making the signal unusable. Since the TEA−IDA gel appeared to be unstable, the infrared spectrum was obtained from the as-synthesized solution. The H_2O-bend at 1630 cm^{-1} dominates the spectrum, hereby masking the possible carboxylate stretching shifts. When comparing this to the spectra of the monometallic Ti−TEA, Sr−IDA, and Ti−IDA precursors (Figure 1a,b,e), it can be seen that the metal-coordinated C−N(−C) stretch is again present at 1112 cm^{-1}, albeit with a lower relative intensity then observed for the monometallic Ti−TEA precursor. This could indicate a ligand exchange at the Ti^{4+} center from coordinated triethanolamine to coordinated iminodiacetic acid. This is further endorsed by the instability of the bimetallic TEA−IDA gel, whereas the monometallic gels of Ti−TEA and Sr−IDA appear to be stable. Due to the ligand exchange, Sr^{2+} ions and triethanolamine remain free in the solution, leading to unstable gels, which is also the case for the monometallic Sr−TEA precursor.

For the TEA−EDTA precursor (Figure 2b), the same fluorescence problem occurred during the Raman measurements. However, despite this fluorescence, a vibration mode can be observed at 630 cm^{-1} which corresponds to the M−O vibration of the Ti−EDTA complex. Again, this would indicate a ligand exchange from triethanolamine to EDTA, which is further confirmed by the presence of characteristic Ti−EDTA vibration modes at 936 cm^{-1}(π(C−O)), 886−868 cm^{-1} (υ(O−O), υ_s(C−N)), and 624 cm^{-1}(υ_{as}(Ti−O_2)). However, despite the presence of a shoulder at 1630 cm^{-1} in the infrared spectrum assigned to the asymmetric coordinated carboxylate stretching of EDTA, also characteristic vibrations of Ti−TEA and Sr−EDTA can be observed at 1110 (υ(C−N(−C))) and 686 cm^{-1}. The presence of these vibrational modes indicates that the ligand exchange is not completed and mixed TEA−EDTA complexes of Ti^{4+} are present in the solution, in combination with EDTA coordinated strontium ions. Moreover, the carboxylate vibrational modes observed at 1580 and 1380 cm^{-1} are clearly shifted with respect to the vibrational modes of the monometallic precursors, indicating that some of EDTA's carboxylate groups are bound to Sr^{2+}. In addition, it cannot be excluded that heteronuclear complexes are formed in which EDTA forms bridges between Sr^{2+} and Ti^{4+} ions. Nevertheless, in all of these situations, it is clear that both the Ti^{4+} and Sr^{2+} are stabilized by the ligands, which can be crucial for the homogeneity of the final products.

In the case of the IDA−IDA precursor, it can be expected that the spectra consist of vibrational motions coming from the organic compounds and the characteristic vibations of the Ti−IDA−H_2O_2 complex, as Sr^{2+} was proven to be unchelated by IDA. Indeed, in Figure 2c the characteristic motions of the Ti−IDA−H_2O_2 complex, which were described previously, are observed in both the infrared and Raman spectrum. It should be noted that broadening or small shifts of the vibrational modes are inherent to matrix effects of these bimetallic precursors, making the spectra more complex to analyze. Nevertheless, the observed vibrations indicate that the Ti^{4+} is stabilized by the ligands, whereas Sr^{2+} remains free in the solution.

The last precursor which was analyzed is obtained by mixing the Sr−EDTA and Ti−IDA precursors. From the vibrational modes observed in the Raman low frequency region in Figure 2d (630, 480, 458, and 406 cm^{-1}), it can be seen that a ligand exchange occurs giving rise to Ti−EDTA chelated sites. The broadening and shift of the asymmetric carboxylate stretch at 1665 cm^{-1} in Raman confirms the ligand exchange, but also indicates the presence of remaining Ti−IDA and Sr−EDTA or heteronuclear complexes. From the fingerprint area of the infrared spectrum, contributions originating from Sr−EDTA (1111 and 714 cm^{-1}), Ti−EDTA (936, 886, and 622 cm^{-1}), and Ti−IDA (1111 and 865 cm^{-1}) can be observed, again leading to the conclusion that both metal ions are stabilized in either a mono- or heteronuclear complex.

In summary, it was shown in the measurements of the monometallic solutions that iminodiacetic acid is incapable of chelating Sr^{2+}, whereas EDTA is able to bond with Sr^{2+} via its nitrogen atoms. Upon adding the strontium solutions to the titanium solution in order to obtain the STO precursor, a ligand exchange was observed leading to an unstable gel for the IDA−TEA solution. For the IDA−IDA solution, only the presence of Ti−IDA−H_2O_2 could be shown, again leaving the Sr^{2+} free in the solution. For the solutions where Sr^{2+} was initially stabilized by EDTA, the ligand exchange also occurred but was not completed, giving rise to either heteronuclear complexes or partially stabilized Sr^{2+}. These differences in strontium stabilization are expected to have a strong influence on the $SrTiO_3$ formation as strontium will be released earlier throughout the thermal processing of the films synthesized from the IDA−IDA and IDA−TEA precursors compared to the precursors where the strontium ions are stabilized by chelation with EDTA.

Despite the differences in precursor chemistry, a similar thermal decomposition behavior is seen for all precursor solutions under air (Figure 3). The weight loss below 200 °C

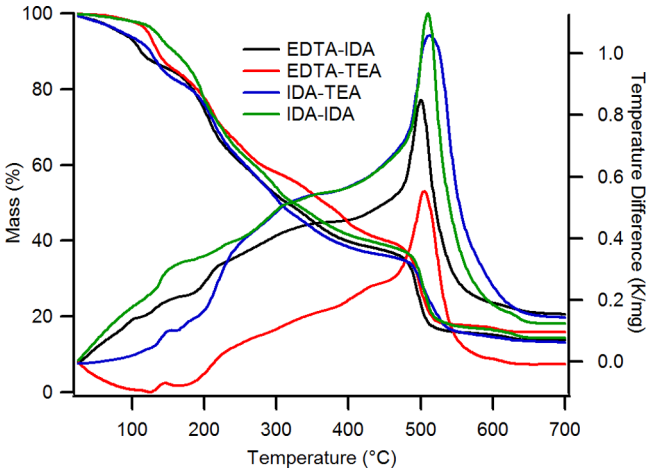

Figure 3. TGA−DTA analysis of the bimetallic precursors performed in flowing air with a heating rate of 10 °C/min.

can be attributed to the vaporization of water, nitric acid, and ethanolamine. The second weight loss between 200 and 480 °C is caused by the decomposition of nitrate groups from the metal precursor, free triethanolamine, and the decarboxylation of free carboxylic acid.[24,26,42] All the solutions exhibit a strong exothermic combustion around 500−510 °C, followed by the removal of residual carbon starting from 600 °C. These final two steps can be assigned to the combustion of the present metal complexes or decoordinated ligands.[29]

dx.doi.org/10.1021/ic403067h | Inorg. Chem. 2014, 53, 4913−4921

3.2. Thin Film Deposition, Growth, and Characterization. In order to study the influence of the precursor chemistry on the growth process and the properties of the films, the solutions were coated onto single crystal $LaAlO_3$ substrates and processed according to the thermal treatment described in the Experimental Section. When processing in dry Ar/5%H_2, epitaxial (200)-oriented films are obtained with only a small fraction of (110) phase present, as shown in the XRD-spectra in Figure 4a. Due to the extremely low oxygen partial

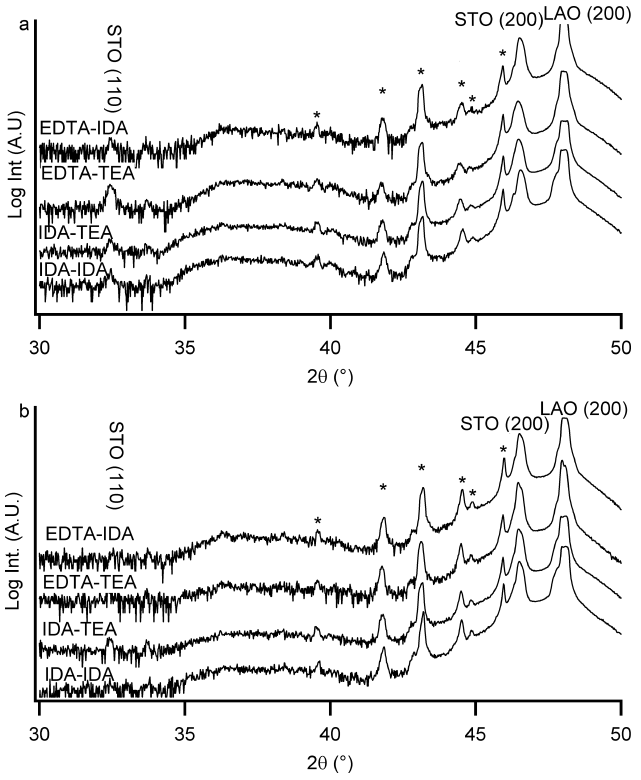

Figure 4. XRD patterns of epitaxial STO films on LAO single crystal substrates obtained in dry (a) and wet (b) processing conditions (reflections marked with an asterisk originate from secondary radiation of the X-ray tube).

pressure ($pO_2 \approx 10^{-17}$ atm) during thermal processing under dry Ar/5% H_2 atmosphere, the combustion of the final complexes is only completed at the sinter-temperature, giving rise to very similar topographical morphologies for the four precursor solutions under investigation (Figure 5). In all cases, it can be seen that there is a worm-like grain structure; however, for the films obtained from the IDA–IDA and EDTA–IDA precursors (Figure 5a,c), also a higher amount of small outgrowths is observed in comparison to the other films. All obtained surfaces appear to be very rough with RMS values higher than 16 nm as determined by AFM (not shown here). The film synthesized from the IDA–TEA precursor shows microscopic inhomogeneities (inset Figure 5b) due to the instability of the gel. Moreover, problems regarding reproducibility are observed for all solutions, occasionally leading to weakly textured films which exhibit a gray to black color.

As shown by XPS measurements (Figure 6), these problems can be attributed to the presence of residual carbon induced by the reducing atmosphere used during processing. As previously shown by other researchers, the presence of residual carbon impedes nucleation and proper grain growth of the ceramic film

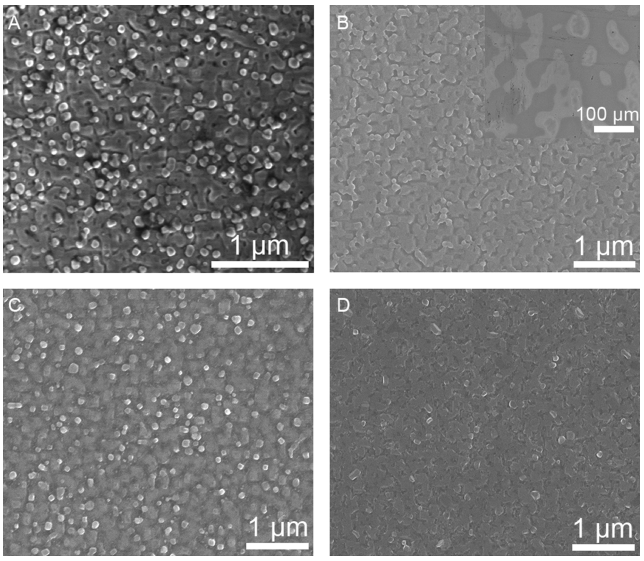

Figure 5. SEM images showing the surface morphology of STO thin films on LAO obtained by dry processing of IDA–IDA (a), IDA–TEA (inset: low magnification) (b), EDTA–IDA (c), and EDTA–TEA (d) precursors.

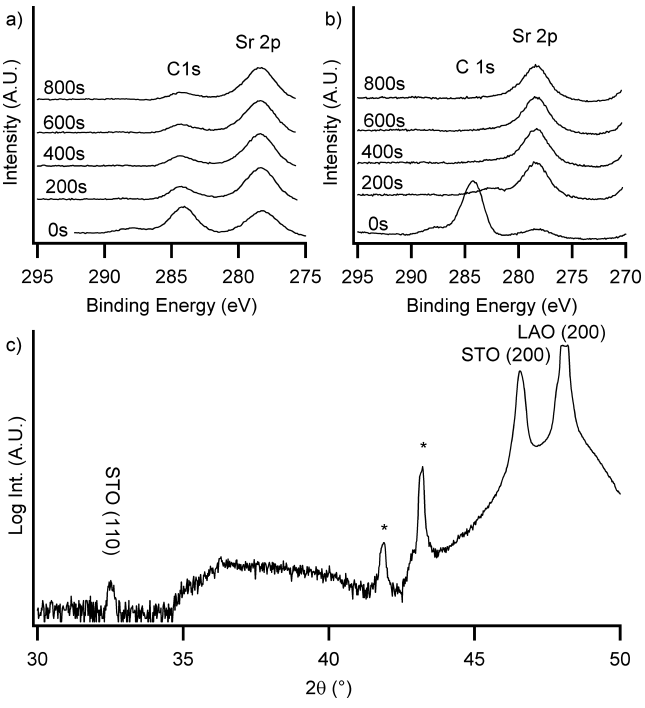

Figure 6. C 1s and Sr 2p binding energy region of films processed in dry Ar/5%H_2 (a) and after oxygen postannealing (b) at different sputtering times; XRD pattern of epitaxial STO films on LAO single crystal substrates obtained after postannealing in oxygen.

during sintering.[43–45] Figure 6 shows the C 1s and Sr 2p binding energy region for films synthesized in dry Ar/5% H_2 and films postannealed in pure oxygen. For both types of processing, surface contamination gives rise to a strong C 1s peak at around 284 eV. However, in the case of processing in dry Ar/5% H_2, the carbon signal only diminishes very slowly after sputtering, indicating the presence of carbon throughout the film. By performing an additional postannealing step in

dx.doi.org/10.1021/ic403067h | Inorg. Chem. 2014, 53, 4913–4921

pure oxygen, the residual carbon is removed, again leading to a strongly textured film as shown in Figure 6c.

Despite the excellent results in terms of residual carbon removal, a postannealing procedure in oxygen is infeasible for further process development as this would give rise to oxidation of the commonly used metallic substrates in coated conductor architectures. Therefore, the oxygen partial pressure was raised ($pO_2 \approx 10^{-14}$ atm) during the synthesis by addition of water vapor to the sinter-atmosphere.[46−48] The XRD spectra in Figure 4b show that all films obtained under these conditions are strongly (200) textured with as good as no (110)-phase present. This indicates that the addition of water vapor to the forming gas improves the texture of the $SrTiO_3$ thin films, which can be attributed to the higher oxygen partial pressure which allows easier growth of the formed nuclei. In contrast to the dry processing conditions, large differences can now be seen regarding morphology between the films obtained via the different precursors.

The SEM images in Figure 7 show that the IDA−TEA and the IDA−IDA solutions give rise to the formation of

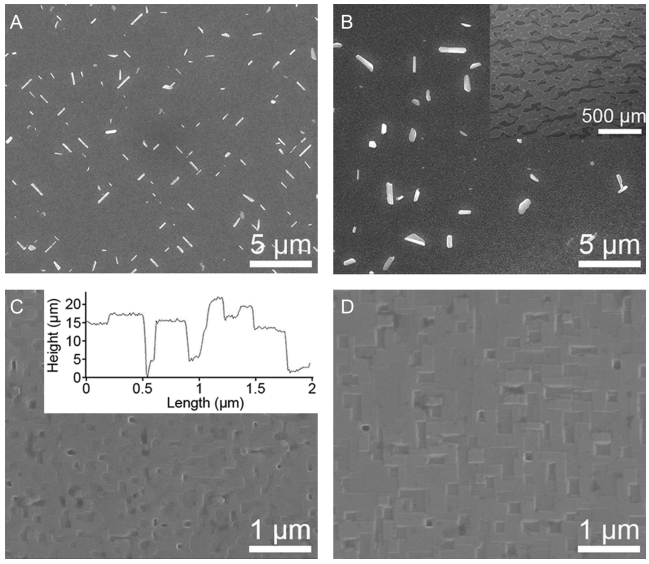

Figure 7. SEM images showing the surface morphology of STO thin films on LAO obtained by wet processing of IDA−IDA (a), IDA−TEA (inset: low magnification) (b), EDTA−IDA (inset: AFM height profile) (c), and EDTA−TEA (d) precursors.

microcrystals on top of the surface, whereas the solutions containing EDTA exhibit uniform and homogeneous surfaces.

The microcrystals observed via SEM were further analyzed by EDX (Figure 8a), from which it can be seen that the microcrystals are strongly Sr-enriched. Prolonged XRD measurements revealed the presence of an additional reflection originating from SrO (111) planes (Figure 8b), confirming the chemical composition of the observed microcrystals. Similar microcrystals have already been observed in literature during the postprocessing of $SrTiO_3$ single crystals and were then identified as either SrO or TiO_x.[49,50] During these treatments, the nature of the crystals depends on the processing conditions, i.e., the atmosphere which is used. For oxidizing treatments, SrO nanocrystal formation is observed, whereas TiO_x crystals are observed when processing in reducing or vacuum conditions. This indicates that the formation of the microcrystals observed here is different in nature than the ones

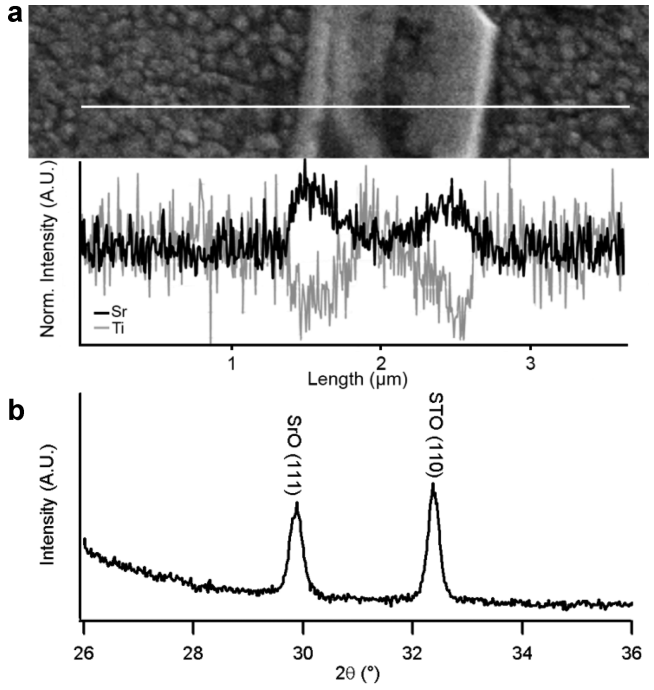

Figure 8. Line scan electron image and normalized intensity plot of Sr and Ti EDX signal (a). XRD pattern of STO films obtained by wet processing of IDA−IDA solution (b).

observed in the literature. The origin of the phase segregation observed in this work is believed to lie in the precursor chemistry of the solutions, described in the previous paragraph. Due to the additional stabilization of Sr^{2+} in the precursors containing EDTA, the STO reaction is controlled by the combustion of both the Sr^{2+} and Ti^{4+} complexes, giving rise to single phase STO films. In the case where Sr^{2+} was initially "stabilized" by IDA, the free strontium ions in the solution are transformed into SrO which is clearly incapable of undergoing complete reaction with TiO_2 or $Sr_{1-x}Ti_{1+y}O_3$, leading to the microcrystals observed in Figures 7 and 8.

Due to the addition of water vapor to the sintering atmosphere, terracing is observed in the solutions containing EDTA (Figure 7 c,d). It is believed that this terracing is a consequence of the facilitated combustion of metal complexes and removal of residual carbon, leading to improved grain growth and better texturing. Given the excellent *a*-axis orientation of the films and the rectangular shape of the terraces, these are believed to be (*h*00)-terminated planes. The microstructure observed in these films is similar to the ones reported by Kunert et al. and Clem et al., showing the high potential of these environmentally friendly precursors.[10,47]

Terracing and stabilization of (100) planes at the surface by the addition of H_2O has already been observed in the case of postannealing sputtered CeO_2 films.[43] The origin of this enhanced terracing due to the presence of water has not been clarified yet, and further research is needed to resolve this phenomenon. The inset of Figure 7c shows the height profile of the formed terraces, revealing a high amount of flat regions. Due to the strong terracing, an RMS roughness of around 12 nm for an area of 25 μm^2 is obtained. Nevertheless, these terraces could be beneficial for subsequent epitaxial layer growth, as the nucleation mechanism can then be supported by the ledges present at the surface.[51] For these reasons, the solutions containing EDTA are believed to be suitable for the

dx.doi.org/10.1021/ic403067h | Inorg. Chem. 2014, 53, 4913−4921

deposition of $SrTiO_3$ thin films in terms of crystallinity and morphology.

As proof of concept, the films obtained by the wet processing of the EDTA−IDA precursor were tested as texture transferring buffer layer by the deposition of YBCO via pulsed laser deposition.[33] Epitaxial growth was observed for the YBCO, giving rise to superior superconducting performances with critical current densities up to 3.6 MA/cm^2 in self-field at 77 K, indicating excellent texture transfer from the $SrTiO_3$ film to the YBCO layer.

4. CONCLUSION

STO thin films were prepared starting from various novel water based precursors. We found that the composition of the precursor solution has a strong influence on the morphology of the ceramic films after thermal processing, especially upon addition of water vapor to the atmosphere. However, these differences in morphology could not be attributed to the thermal decomposition behavior of the solutions, as all the solutions showed similar behavior upon heating. Thorough precursor analysis via Raman and infrared spectroscopy however showed that, in some cases, depending on the type of chelating agent chosen for Ti^{4+} and Sr^{2+}, respectively, the Sr^{2+} ions remain free in solution after mixing of the precursors, leading to undesired reactions during thermal processing. Therefore, it is clear that the stabilization of Sr^{2+} is crucial in order to obtain single phase, highly textured $SrTiO_3$ films. Next to this, we were able to show that the introduction of water vapor in the synthesis atmosphere yields a strong increase in biaxial texture for all films. Nevertheless, if strontium was not stabilized in the precursor solution, microcrystal formation was observed on the surface of the films. Only precursors where both metal ions were stabilized in combination with a wet thermal treatment gave rise to strongly textured, dense, and terraced $SrTiO_3$ films. Their excellent crystallographic and morphological properties were demonstrated by the deposition of epitaxial YBCO on top of the synthesized $SrTiO_3$ films, leading to superior superconducting performances. In general, it can be stated that only solutions in which both metal ions are stabilized appear to be suitable for single phase $SrTiO_3$ formation and the deposition of films which are capable of meeting the requirements for further usage in applications.

■ ASSOCIATED CONTENT

Supporting Information

Assignment of the various absorption bands and Raman shifts. This material is available free of charge via the Internet at http://pubs.acs.org.

■ AUTHOR INFORMATION

Corresponding Author

*E-mail: Isabel.VanDriessche@UGent.be. Phone: +32(0) 92644550, +32(0)92644433. Fax: +32(0)9 264 49 83.

Notes

The authors declare no competing financial interest.

■ ACKNOWLEDGMENTS

One of the authors (G.P.) would like to thank the Institute for the Promotion of Innovation through Science and Technology in Flanders (IWT) for funding. The authors would like to thank Olivier Janssens for XRD analysis, Dr. Els Bruneel for XPS analysis, and Dr. Ruben Hühne of IFW Dresden for PLD-YBCO deposition. Part of this work was performed within the framework of the EuroTapes project (FP7-NMP.2011.2.2-1 Grant 280438), funded by the European Union.

■ REFERENCES

(1) Bibes, M.; Villegas, J. E.; Barthelemy, A. *Adv. Phys.* **2011**, *60* (1), 5−84.
(2) Gao, Y. F.; Masuda, Y.; Yonezawa, T.; Koumoto, K. *Mater. Sci. Eng., B* **2003**, *99* (1−3), 290−293.
(3) Hasenkox, U.; Hoffmann, S.; Waser, R. *J. Sol-Gel Sci. Technol.* **1998**, *12* (2), 67−79.
(4) Hoffmann, S.; Waser, R. *J. Eur. Ceram. Soc.* **1999**, *19* (6−7), 1339−1343.
(5) Schwartz, R. W.; Clem, P. G.; Voigt, J. A.; Byhoff, E. R.; Van Stry, M.; Headley, T. J.; Missert, N. A. *J. Am. Ceram. Soc.* **1999**, *82* (9), 2359−2367.
(6) Siegal, M. P.; Clem, P. G.; Dawley, J. T.; Ong, R. J.; Rodriguez, M. A.; Overmyer, D. L. *Appl. Phys. Lett.* **2002**, *80* (15), 2710−2712.
(7) Kakihana, M.; Okubo, T.; Arima, M.; Nakamura, Y.; Yashima, M.; Yoshimura, M. *J. Sol-Gel Sci. Technol.* **1998**, *12* (2), 95−109.
(8) Pollefeyt, G.; Rottiers, S.; Vermeir, P.; Lommens, P.; Huhne, R.; De Buysser, K.; Van Driessche, I. *J. Mater. Chem. A* **2013**, *1* (11), 3613−3619.
(9) Van Driessche, I.; Feys, J.; Hopkins, S. C.; Lommens, P.; Granados, X.; Glowacki, B. A.; Ricart, S.; Holzapfel, B.; Vilardell, M.; Kirchner, A.; Backer, M. *Supercond. Sci. Technol.* **2012**, *25* (6), 065017.
(10) Kunert, J.; Backer, M.; Brunkahl, O.; Wesolowski, D.; Edney, C.; Clem, P.; Thomas, N.; Liersch, A. *Supercond. Sci. Technol.* **2011**, *24* (8), 085018.
(11) Eisenbeiser, K.; Finder, J. M.; Yu, Z.; Ramdani, J.; Curless, J. A.; Hallmark, J. A.; Droopad, R.; Ooms, W. J.; Salem, L.; Bradshaw, S.; Overgaard, C. D. *Appl. Phys. Lett.* **2000**, *76* (10), 1324−1326.
(12) Panomsuwan, G.; Cho, S. P.; Saito, N.; Takai, O. *Cryst. Res. Technol.* **2012**, *47* (2), 187−194.
(13) McKee, R. A.; Walker, F. J.; Chisholm, M. F. *Phys. Rev. Lett.* **1998**, *81* (14), 3014−3017.
(14) Wang, H.; Foltyn, S. R.; Arendt, P. N.; Jia, Q. X.; Li, Y.; Zhang, X. *Physica C* **2005**, *433* (1−2), 43−49.
(15) Obradors, X.; et al. *Supercond. Sci. Technol.* **2006**, *19* (3), S13−S26.
(16) Schwartz, R. W. *Chem. Mater.* **1997**, *9* (11), 2325−2340.
(17) Wang, Y.; Zhou, L.; Li, C. S.; Yu, Z. M.; Li, J. S.; Jin, L. H.; Shen, Y.; Wang, P. F.; Lu, Y. F. *J. Mater. Sci.* **2012**, *47* (1), 433−439.
(18) Kakihana, M.; Kobayashi, M.; Tomita, K.; Petrykin, V. *Bull. Chem. Soc. Jpn.* **2010**, *83* (11), 1285−1308.
(19) Hardy, A.; D'Haen, J.; Van Bael, M. K.; Mullens, J. *J. Sol-Gel Sci. Technol.* **2007**, *44* (1), 65−74.
(20) Arin, M.; Lommens, P.; Avci, N.; Hopkins, S. C.; De Buysser, K.; Arabatzis, I. M.; Fasaki, I.; Poelman, D.; Van Driessche, I. *J. Eur. Ceram. Soc.* **2011**, *31* (6), 1067−1074.
(21) Lommens, P.; Bruggeman, T.; Pollefeyt, G.; Arin, M.; Feys, J.; Van Driessche, I. *MRS Online Proc. Libr.* **2012**, *1454*, 209−214.
(22) Cloet, V.; Lommens, P.; Huhne, R.; De Buysser, K.; Hoste, S.; Van Driessche, I. *J. Cryst. Growth* **2011**, *325* (1), 68−75.
(23) Narayanan, V.; Lommens, P.; De Buysser, K.; Huhne, R.; Van Driessche, I. *J. Solid State Chem.* **2011**, *184* (11), 2887−2896.
(24) Van de Velde, N.; Bruggeman, T.; Stove, L.; Pollefeyt, G.; Brunkahl, O.; Van Driessche, I. *Eur. J. Inorg. Chem.* **2012**, *8*, 1186−1194.
(25) Penneman, G.; Van Driessche, I.; Bruneel, E.; Hoste, S. *Deposition of CeO_2 Buffer Layers and $YBa_2Cu_3O_{7-\sigma}$ Superconducting Layers Using an Aqueous Sol-Gel Method*; Mandal, H, Ovecoglu, L, Eds.; Euro Ceramics Viii, Pts 1−3; Trans Tech Publications Ltd: Zurich-Uetikon, 2004; pp 501−504.
(26) Feys, J.; Vermeir, P.; Lommens, P.; Hopkins, S. C.; Granados, X.; Glowacki, B. A.; Baecker, M.; Reich, E.; Ricard, S.; Holzapfel, B.; Van der Voort, P.; Van Driessche, I. *J. Mater. Chem.* **2012**, *22* (9), 3717−3726.

(27) Vermeir, P.; Cardinael, I.; Schaubroeck, J.; Verbeken, K.; Backer, M.; Lommens, P.; Knaepen, W.; D'Haen, J.; De Buysser, K.; Van Driessche, I. *Inorg. Chem.* **2010**, *49* (10), 4471−4477.
(28) Bu, S. J.; Jin, Z. G.; Liu, X. X.; Yang, L. R.; Cheng, Z. J. *J. Eur. Ceram. Soc.* **2005**, *25* (5), 673−679.
(29) De Dobbelaere, C.; Mullens, J.; Hardy, A.; Van Bael, M. K. *Thermochim. Acta* **2011**, *520* (1−2), 121−133.
(30) Hardy, A.; Gielis, S.; Van den Rul, H.; D'Haen, J.; Van Bael, M. K.; Mullens, J. *J. Eur. Ceram. Soc.* **2009**, *29* (14), 3007−3013.
(31) Van Driessche, I.; Penneman, G.; De Meyer, C.; Stambolova, I.; Bruneel, E.; Hoste, S. *The Influence of Sol Gel Precursors and Substrate Type in the Spin Coating of CeO_2 Thin Films*; Euro Ceramics Vii, Pt 1−3; Trans Tech Publications Ltd.: Zurich-Uetikon, 2002; pp 479−482.
(32) Vermeir, P.; Deruyck, F.; Feys, J.; Lommens, P.; Schaubroeck, J.; Van Driessche, I. *J. Sol-Gel Sci. Technol.* **2012**, *62* (3), 378−388.
(33) Huhne, R.; Selbmann, D.; Eickemeyer, J.; Hanisch, J.; Holzapfel, B. *Supercond. Sci. Technol.* **2006**, *19* (2), 169−174.
(34) Horcas, I.; Fernandez, R.; Gomez-Rodriguez, J. M.; Colchero, J.; Gomez-Herrero, J.; Baro, A. M. *Rev. Sci. Instrum.* **2007**, *78* (1), 013705.
(35) Nakamoto, K. *Infrared and Raman Spectra of Inorganic and Coordination Compounds Part B: Applications in Coordination, Organometallic and Bioinorganic Chemistry*; John Wiley & Sons Inc.: New York, 1997.
(36) Baran, E. J.; Wagner, C. C.; Torre, M. H. *J. Braz. Chem. Soc.* **2002**, *13* (5), 576−582.
(37) Fiorucci, A. R.; de Paula, L. R.; Neves, E. A.; Cavalheiro, E. T. G. *J. Chem. Eng. Data* **2002**, *47* (6), 1510−1513.
(38) Anderegg, G. *Helv. Chim. Acta* **1964**, *47* (7), 1801.
(39) Sigel, H.; Scheller, K. H.; Prijs, B. *Inorganica Chimica Acta-Bioinorganic Chemistry* **1982**, *66* (5), 147−155.
(40) Stetter, H.; Frank, W.; Mertens, R. *Tetrahedron* **1981**, *37* (4), 767−772.
(41) Martell, A. E.; Smith, R. M. *Critical Stability Constants*; Plenum Press: New York, 1975.
(42) Nelis, D.; Mondelaers, D.; Vanhoyland, G.; Hardy, A.; Van Werde, K.; Van den Rul, H.; Van Bael, M. K.; Mullens, J.; Van Poucke, L. C.; D'Haen, J. *Thermochim. Acta* **2005**, *426* (1−2), 39−48.
(43) Pomar, A.; Coll, M.; Cavallaro, A.; Gazquez, J.; Mestres, N.; Sandiumenge, F.; Puig, T.; Obradors, X. *J. Mater. Res.* **2006**, *21* (9), 2176−2184.
(44) Coll, M.; Gazquez, J.; Sandiumenge, F.; Puig, T.; Obradors, X.; Espinos, J. P.; Huhne, R. *Nanotechnology* **2008**, *19* (39), 395601.
(45) Augieri, A. *IEEE Trans. Appl. Supercond.* **2013**, *23* (3), 6600505.
(46) Venkataraman, K.; Hellstrom, E. *J. Mater. Res.* **2009**, *24* (4), 1567−1575.
(47) Clem, P. G.; Dawley, J. T.; Siegal, M. P.; Overmyer, D. L.; Richardson, J. J.; Voigt, J. A.; Holesinger, T. A. *Int. J. Appl. Ceram. Technol.* **2005**, *2* (1), 24−32.
(48) Rupich, M. W.; Schoop, U. D.; Verebelyi, D.; Kodenkandath, T.; Li, X. (American Superconductor Corporation). Deposition of Buffer Layers on Textured Metal Surfaces, 2007. Patent No. US007261776B2.
(49) Szot, K.; Speier, W.; Breuer, U.; Meyer, R.; Szade, J.; Waser, R. *Surf. Sci.* **2000**, *460* (1−3), 112−128.
(50) Lee, S. B.; Phillipp, F.; Sigle, W.; Ruhle, M. *Ultramicroscopy* **2005**, *104* (1), 30−38.
(51) Xu, Y.; Goyal, A.; Lian, J.; Rutter, N. A.; Shi, I.; Sathyamurthy, S.; Paranthaman, M.; Wang, L.; Martin, P. M.; Kroeger, D. M. *J. Am. Ceram. Soc.* **2004**, *87* (9), 1669−1676.